KFUPM
Journal of Undergraduate Research International

Diamond Open Access 109

Article Geosciences

Hydrothermal Alteration of Quartz-rich Glass Sand and Its Implications for Reservoir Quality Evolution

Ayah Alkhalifah and Anas Muhammad Salisu*

Cite https://doi.org/10.64589/juri/231553

Submitted: April 28, 2026 **Revised:** May 03, 2026 **Accepted:** May 04, 2026

ABSTRACT

Quartz-rich sandstones are considered chemically stable during burial diagenesis; however, even minor reactive mineral fractions can considerably influence their evolution, and the extent to which these minor components drive diagenetic processes in quartz-rich sands remains insufficiently understood. Therefore, we investigated the hydrothermal alteration of quartz-rich glass sand from the Middle Jurassic Mariedal Formation in Sweden. We conducted a series of 14-day-long batch experiments at temperatures of 80, 150, 200, and 250 °C using natural Red Sea water as the reacting fluid. The starting material was dominated by quartz (>93%), with minor amounts of K-feldspar and muscovite providing limited but sufficient sources of the reactive components. Feldspar dissolution was initiated at low temperatures, progressively releasing the key elements required for clay mineral formation. Authigenic smectite first developed at 150 °C as discontinuous grain-coating phases, becoming more extensive at 200 °C and subsequently transforming into illite at 250 °C. Fluid chemistry trends show decreasing Mg^{2+} and increasing Fe^{3+} and K^{+} concentrations with temperature, indicating strong coupling between mineral reactions and element redistribution. These results demonstrate that quartz-rich sands are not chemically inert and can undergo significant mineralogical transformations under the appropriate thermal and fluid conditions. Overall, this study provides experimental insights into clay mineral evolution in quartz-rich systems and highlights the critical role of coupled mineral–fluid interactions in controlling reservoir quality during burial diagenesis.

Keywords: glass sand; hydrothermal experiments; quartz; smectite, illite; reservoir quality

1. INTRODUCTION

Quartz-rich sandstones constitute a major component of many hydrocarbon reservoirs and are commonly associated with relatively high initial porosity and permeability [1–4]. Their diagenetic evolution is interpreted as being primarily controlled by mechanical compaction and quartz cementation, with limited emphasis on chemical alteration processes [5]. However, growing evidence indicates that even in quartz-dominated systems, subtle mineral reactions can substantially influence reservoir evolution [6]. In particular, the presence of minor reactive minerals, such as feldspar and mica, can introduce pathways for chemical alteration that are not readily apparent from the bulk composition alone. However, the extent to which these minor components drive diagenetic processes in quartz-rich sands remains insufficiently understood.

Hydrothermal alteration experiments provide an effective framework for simulating the early-to-intermediate stages of burial diagenesis under controlled laboratory conditions [7–9]. Such experiments enable the investigation of mineral transformations that would otherwise occur over geological timescales by accelerating temperature-dependent reactions. This approach is particularly valuable for understanding how fluid–rock interactions influence mineral stability, elemental mobility, and the formation of secondary phases. However, most experimental studies have focused on clay-rich or feldspathic systems, leaving quartz-rich sand relatively unexplored.

An important outcome of fluid–rock interactions in siliciclastic systems is the formation of authigenic clay minerals [10,11]. These minerals can occur as grain coatings or pore-filling phases, playing a critical role in modifying pore structure and permeability [12]. In quartz-rich sands, clay mineral development is often underestimated because of the dominance of quartz; however, even small amounts of reactive minerals can supply the elements necessary for clay precipitation [13,14]. The formation of smectite and its subsequent transformation into illite represents a key diagenetic pathway with contrasting implications for reservoir quality [15,16]. Although smectite can preserve porosity under certain conditions, illite is commonly associated with permeability reduction owing to pore-throat blockage [17,18]. Despite their importance, the mechanisms that control clay mineral formation and transformation in quartz-rich systems remain poorly understood.

In this context, we investigated the hydrothermal alteration of quartz-rich glass sand from the Middle Jurassic Mariedal Formation in Sweden. Unlike conventional studies that have focused on more reactive sedimentary systems, we examined the response of a nearly pure quartz framework to elevated temperatures and reactive fluids. The main objective was to evaluate how mineral

Published under an exclusive license by KFUPM

Table 1. *Hydrothermal experimental conditions*

Experiment	Sample ID	Solutions	Temperature (°C)	Duration (Days)
1	GL1	Red Sea water	80	14
2	GL2	Red Sea water	150	14
3	GL3	Red Sea water	200	14
4	GL4	Red Sea water	250	14

transformations in such a system influence the evolution of reservoir quality. Specifically, we (1) assessed the extent of mineral alteration in quartz-rich sand under hydrothermal conditions, (2) identified the formation and transformation of clay minerals, and (3) examined the relationship between mineral evolution and fluid chemistry. By integrating mineralogical observations with fluid geochemistry, this study provides a process-based experimental analog for diagenetic alterations in quartz-rich sandstones. The results offer new insights into how seemingly stable reservoir systems can undergo substantial transformations and highlight the importance of fluid–rock interactions in predicting reservoir behavior during burial diagenesis.

2. MATERIALS AND METHODS

2.1. Starting Material. Our starting material was quartz-rich glass sand from the Middle Jurassic Mariedal Formation in the Eriksdal/Fyledalen quarry, southern Sweden. Commonly referred to as the Glass Sand Member, this unit is predominantly composed of well-sorted medium-grained quartz sand with characteristic cross-bedding, occasional heavy mineral concentrations, and ferruginous concretions [19,20]. The sediment has an exceptionally high silica content (exceeding 99%) and has historically been exploited as a raw material for industrial glass production.

2.2. Experimental Procedure. To simulate diagenetic conditions, a series of hydrothermal experiments were conducted under controlled laboratory settings using the protocol established in [9,17,21,22]. The experiments were performed using a multiposition stirred autoclave system with closed-system conditions (Figure 1). In each experiment, a fixed 20-g mass of glass sand was reacted with 200 mL of natural Red Sea water to maintain a consistent fluid-to-solid ratio throughout the study. Prior to heating, the reactors were sealed and pressurized with nitrogen to establish initial conditions representative of subsurface environments. Then, the samples were heated at a controlled rate to target temperatures of 80, 150, 200, and 250 °C and maintained under these conditions for 14 days. As the system was closed, the internal pressure increased during heating and varied with the temperature (Table 1). After each experimental run, the reactors were cooled to room temperature before opening. The solid samples were retrieved, dried under ambient conditions, and prepared for further analysis. Coexisting fluids were collected immediately, and their physicochemical properties were measured to assess the changes resulting from mineral reactions.

2.3. Analytical Techniques. Petrographic, mineralogical, and geochemical techniques were employed to characterize the starting material and experimental products. The initial characterization of the sand was performed using conventional thin-section petrography under transmitted light, allowing the identification of framework grains, grain contacts, and preexisting mineral coatings. The changes in the grain surface texture and mineral morphology were investigated using scanning electron microscopy (SEM) coupled with energy-dispersive spectroscopy (EDS). This technique provides detailed imaging of mineral surfaces and enables the identification of newly formed authigenic phases and their chemical compositions.

Bulk mineralogical and chemical changes were further quantified using X-ray diffraction (XRD) and wavelength-dispersive X-ray fluorescence (WD-XRF). XRD analyses were performed on both bulk samples and the <2-μm clay fraction to determine mineral phases and track the development of clay minerals. The clay fraction was separated using standard dispersion, settling, and centrifugation methods and analyzed under different treatment conditions to distinguish between expandable and nonexpandable clay species. WD-XRF analyses were used to determine the bulk chemical composition of the samples, providing insight into element redistribution during the experiments.

In addition, fluid samples collected after each experiment were analyzed using inductively coupled plasma–optical emission spectroscopy (ICP-OES) to determine the concentrations of the major cations. These measurements are essential for evaluating fluid–rock interactions and identifying trends in element mobility and uptake during mineral transformation. Detailed procedures and methodology used in this study are presented previously [9,23,24].

3. RESULTS

3.1. Analytical Techniques. Petrographic observations showed that the starting material was dominated by medium- to coarse-grained framework grains that were primarily subangular to sub-rounded (Figure 2a). Quartz was the main detrital component, whereas K-feldspar, muscovite, aragonite, and minor accessory phases occurred in significantly lower proportions (Figure 2a–c). SEM observations confirmed the clean quartz-dominated character of the starting sand (Figure 2b). Most grains showed angular-to-subangular outlines, local microfractures, and small attached fine particles. The EDS spectra of the dominant framework grains were composed of Si and O, consistent with a quartz composition (Figure 2c).

Bulk geochemical analysis confirmed the Si-rich nature of the starting material. SiO_2 is the dominant oxide, with subordinate amounts of Al_2O_3, K_2O, CaO, Fe_2O_3, and TiO_2 (Table 2; Figure 3). Bulk XRD analysis further showed that the starting material was primarily quartz (>93%) with minor amounts of K-feldspar (4 %), muscovite, and aragonite (Figure 4). The <2-μm fraction contained only a small amount of quartz, and no smectite, illite,

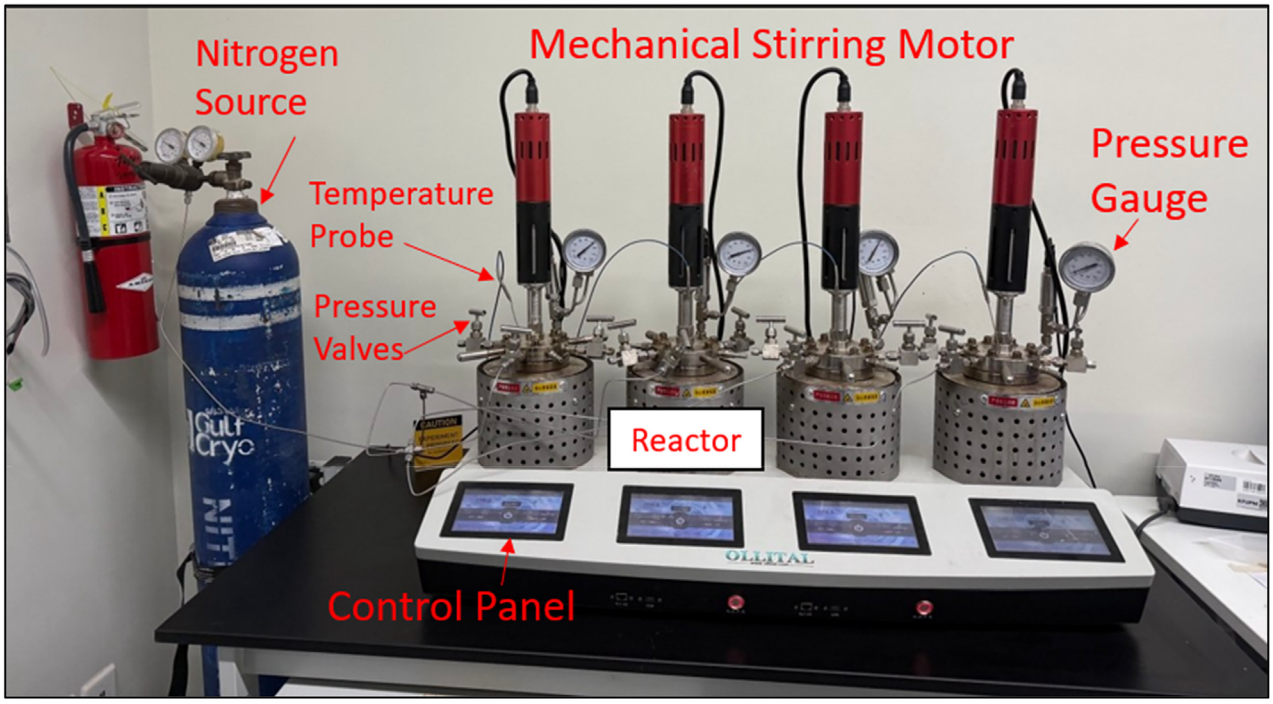


Figure 1. Experimental setup. The system consists of four multi-position reactors with kettles in parallel, each capable of holding up to 500 mL of solution. The reactors can be heated to a maximum temperature of 350 °C and hold pressures of 160 bar

or mixed-layer clay phases were detected prior to hydrothermal treatment (Table 3).

3.2. Temperature Dependent Mineral Alteration.

The hydrothermal experiments produced systematic mineralogical and geochemical changes with increasing temperature. Although quartz remained the dominant mineral phase in all reacted samples, the relative abundances of K-feldspar and muscovite decreased progressively with increasing experimental temperature (Figure 4). Specifically, K-feldspar decreased from 4% in the starting material to 0.6% at 250 °C. Aragonite also decreased with increasing temperature and was not detected in the higher-temperature experiments. This trend indicates the progressive dissolution or alteration of minor reactive minerals within quartz-rich sand. Bulk XRD analysis showed that the reacted samples remained quartz-dominated throughout the temperature series (Table 3, Figure 4). The quartz content

Table 2. *Wavelength-dispersive X-ray fluorescence (WD-XRF) analysis results of the starting material and post-reacted samples (SM, starting material)*

Identification		**Major and Minor Elements (wt%)**										
Experiment	Sample ID	SiO_2	Al_2O_3	K_2O	CaO	MgO	Na_2O	Fe_2O_3	Cl_2O_7	TiO_2	ZrO_2	CoO
SM	GL0	85.98	2.01	5.21	0.37	0.00	0.04	0.90	3.00	1.49	0.11	0.06
Exp. 1	GL1	83.46	1.73	4.84	0.94	0.02	0.29	2.31	1.03	1.97	2.09	0.14
Exp. 2	GL2	81.30	1.58	3.85	1.27	0.04	0.29	1.70	6.72	0.84	0.14	0.11
Exp. 3	GL3	81.31	2.60	2.60	0.26	0.42	0.43	2.70	7.60	0.74	0.13	0.13
Exp. 4	GL4	84.22	2.28	2.49	0.35	0.86	2.09	4.31	1.96	0.50	0.14	0.00

Table 3. *Bulk and clay fraction compositions, with percentage clay fraction, in pre-and post-reacted samples*

Bulk Minerology (%)						**Clay Minerology (<2 µm) (%)**		
Sample ID	**Qtz**	**Mic**	**Mus**	**Arg**	**CM**	**Sme**	**Ill**	**Qtz**
GL0	93.3	4.2	1.4	1.1	0	ND	ND	3.4
GL1	93.9	3.9	1.3	0.9	0	ND	ND	1.3
GL2	94.3	2.9	0.4	0.7	1.7	93.2	5.4	1.4
GL3	94.6	1.9	0.4	0	3.1	54.7	43.9	1.4
GL4	95.1	0.6	0.2	0	4.1	24.7	75.1	0.2

Qtz: quartz; Mic: muscovite; Arg: aragonite; CM: clay minerals; Sme: smectite; and Ill: illite.

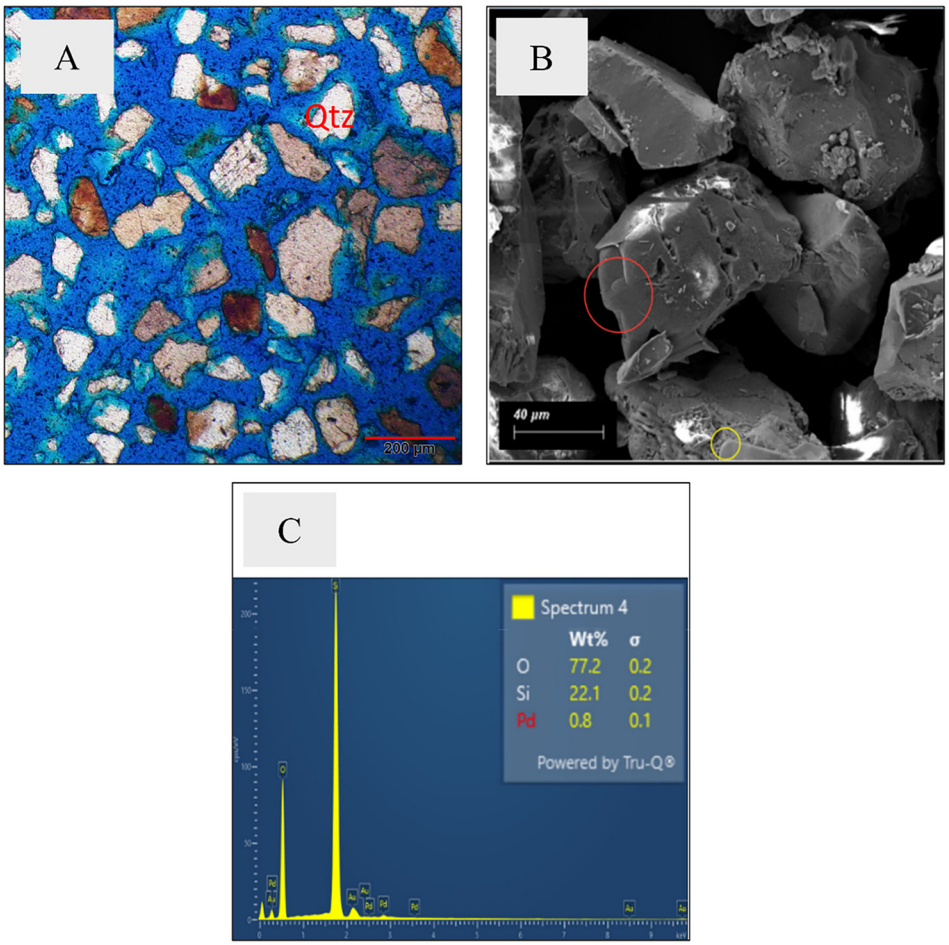


Figure 2. Petrographic images showing the framework grains and detrital grain-coating minerals of the starting material. (a) Thin-section micrograph showing the distribution of the detrital grains, with quartz (Qtz) as the most dominant component of the glass sand. (b) Scanning electron microscopy (SEM) image showing angular detrital grains with surface microfractures and adhered fine particles. Note the absence of any grain-coating clay in the starting material. (c) Energy-dispersive spectroscopy (EDS) spectrum of silicate-rich grains dominated by O and Si, indicating quartz (Qtz) composition, location of which is denoted by the red circle in (b)

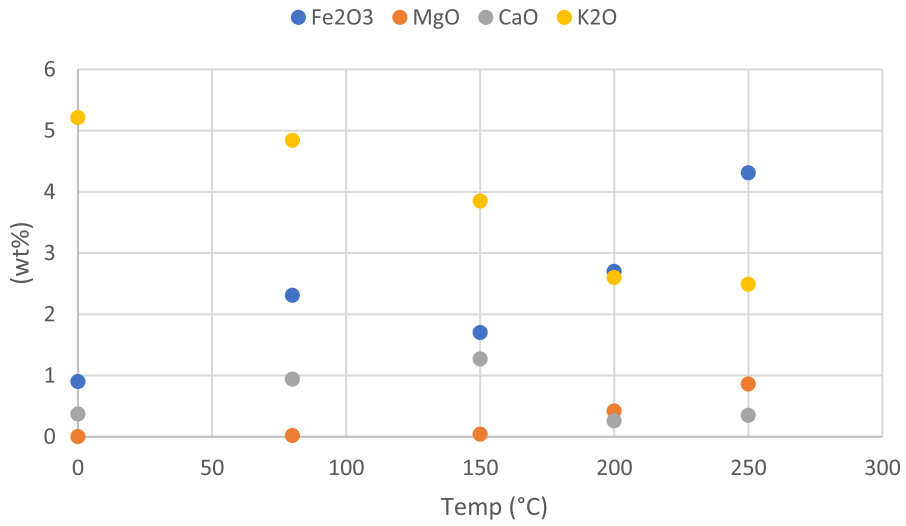


Figure 3. Wavelength-dispersive X-ray fluorescence (WD-XRF) concentrations for Fe_2O, MgO, CaO, and K_2O versus experimental temperatures illustrating their evolution as temperature increases during the hydrothermal experiments

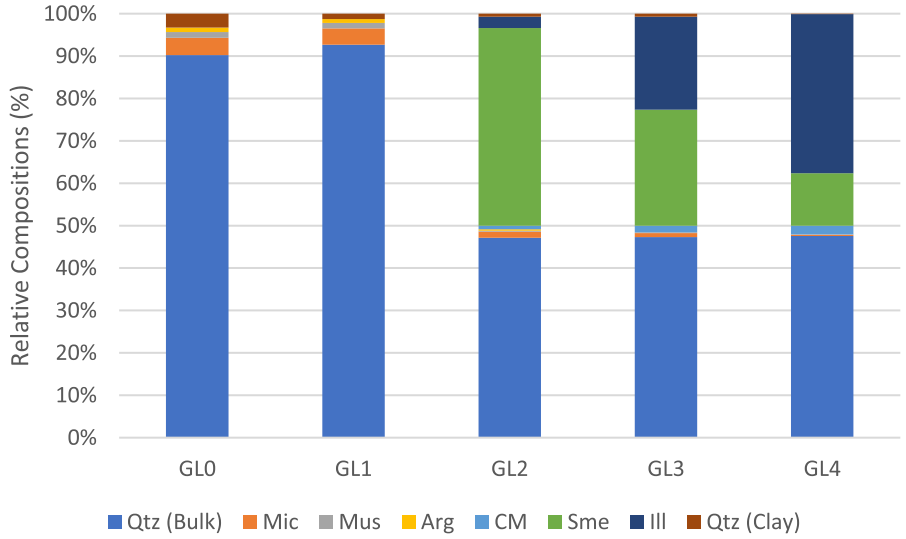


Figure 4. X-ray diffraction (XRD) patterns of clay (<2μm) samples GL0, GL1, GL2, GL3 and GL4 showing quartz as the dominant crystalline phase, along with microcline, muscovite, illite, smectite, and aragonite

increased slightly from approximately 93% in the starting material to approximately 95% in the highest-temperature product, reflecting the continued dominance of the quartz framework and the relative decline of the less stable minor phases.

The WD-XRF results supported these mineralogical trends (Table 2, Figure 3). SiO_2 remained the dominant oxide in all samples, but oxide composition varied with temperature. K_2O decreased steadily from the lower-temperature to higher-temperature products, consistent with the progressive alteration of K-bearing minerals (Figure 3). In contrast, Fe_2O_3 and MgO increased in abundance in the higher-temperature experiments, suggesting enrichment of Fe^{3+} and Mg^{2+} in newly formed alteration products (Figure 3). Al_2O_3 exhibited a slight increase at higher temperature, whereas CaO varied with an overall decreasing trend except for minor fluctuations (Table 2).

3.3. Development of Authigenic Clay Minerals and Textural Evolution. Clay-fraction XRD (Table 3) revealed that clay mineral formation began only after the hydrothermal treatment reached a moderate temperature. In the starting sample and 80 °C product, smectite and illite were not detected. Thus, the low-temperature alteration is mainly limited to the early dissolution of reactive grains rather than measurable clay precipitation. At 80 °C, SEM observations (Figure 5a–b) show that alteration is limited to localized surface corrosion, microcline fragmentation, and early dissolution textures. No continuous authigenic clay coatings were observed at this stage, indicating that the reaction had not yet reached conditions favorable for clay precipitation. At 150 °C (Table 3), smectite first appeared in the <2-μm fraction, representing the main newly formed clay phase (Table 3). SEM observations show that fine-grained clay coatings began to nucleate on the detrital grain surfaces. These coatings were discontinuous and occurred mainly as thin patches, suggesting the development of early stage authigenic clay (Figure 6). The EDS spectra of these coatings show Al-, Mg-, and Fe-bearing aluminosilicate compositions consistent with authigenic smectite (Figure 6). This stage marks the transition from simple mineral dissolution to the formation of active clay minerals.

At 200 °C, smectite became more abundant and formed thicker coatings on grain surfaces (Figure 7a). SEM images show widespread clay coverage and local honeycomb-like textures typical of smectitic clay (Figure 7a–d). The clay fraction XRD analysis also indicated the presence of both smectite and illite, suggesting the onset of clay transformation (Table 3). Therefore, the reacted sand at this stage recorded both continued smectite growth and the beginning of illitization. At 250 °C, the clay assemblage changed significantly (Figure 7c–d). Illite had become the dominant clay mineral in the <2-μm fraction (Table 3), though smectite remained present in lower abundance. SEM images show platy and stacked clay aggregates consistent with the illite morphology (Figure 8a–b). EDS analyses indicated the existence of Al- and K-bearing aluminosilicate compositions, supporting the identification of illite-rich clay phases (Figure 8d). This progression indicates that the hydrothermal alteration of the glass sand followed a clear temperature-dependent pathway from feldspar dissolution to smectite formation and finally to illite development.

3.4. Fluid Chemistry During Hydrothermal Alteration. The chemistry of the reacting fluids changed significantly with increasing temperature. The starting Red Sea water had an alkaline pH of 8.1, but the post-reaction fluids became acidic, with pH values between 3.9 and 4.3. This shift indicates active fluid–rock interactions during the experiments (Table 4). Dissolved Fe increased significantly with temperature. This trend indicates enhanced Fe release or mobilization during high-temperature alteration. In contrast, dissolved Mg^{2+} decreased throughout the experiments, suggesting progressive uptake of Mg^{2+} into newly formed clay minerals, particularly smectite. Dissolved K^+ increased with temperature, reaching its highest value at 250 °C . This increase is consistent with the dissolution of K-bearing minerals, such as K-feldspar and muscovite. The availability of K^+ at higher temperatures supports the transformation of smectite into illite. Ca showed variable behavior but reached its highest concentration at 250 °C, indicating continued

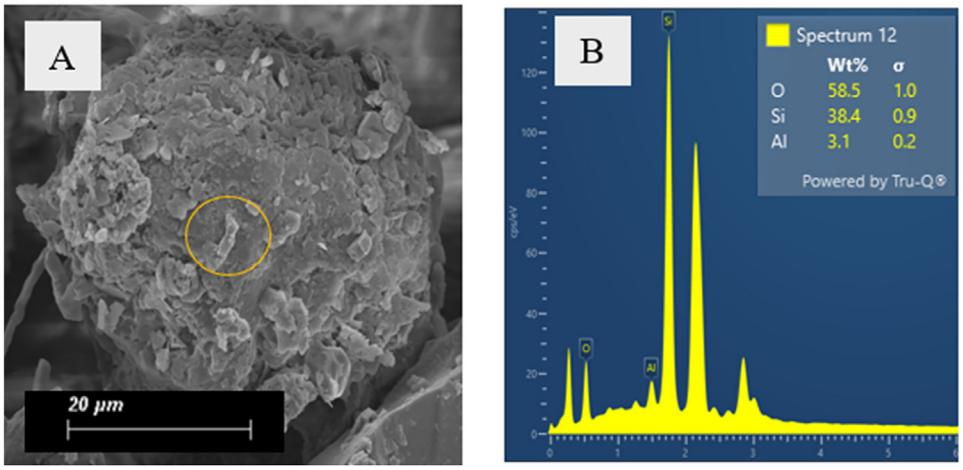


Figure 5. Scanning electron microscopy (SEM) and energy-dispersive spectroscopy (EDS) images displaying diagenetic features observed in Experiment 1 (80 °C). (a) SEM image of feldspar breaking into fragments. (*b*) EDS spectrum of the clay-rich area (yellow circle in a) indicating a Si–O–Al–dominated composition consistent with feldspar minerals

redistribution of soluble components during hydrothermal alteration. Overall, fluid chemistry confirmed that mineral alteration was accompanied by active element exchange between the solid and fluid phases. The combined mineralogical, textural, and geochemical results indicate that quartz-rich glass sand underwent progressive hydrothermal alteration, beginning with the dissolution of minor reactive minerals, followed by smectite coating development, and finally temperature-controlled illitization.

4. DISCUSSION

4.1. Mineral Reactivity in Quartz-rich Systems.

The results demonstrate that, despite its high silica content, quartz-rich glass sand is not chemically inert under hydrothermal conditions. Although quartz remained the dominant phase throughout the experiments, the progressive reduction of K-feldspar and muscovite highlights the critical role of these minor constituents in controlling the system reactivity. Their dissolution releases key elements, including Si, Al, and K, which are essential for the formation of secondary minerals. This indicates that the geochemical evolution of the system was governed by the behavior of the reactive minority phases and not by the dominant quartz framework.

Observed at 80 °C, the earliest stage of alteration is characterized by localized feldspar corrosion and grain-surface destabilization. This demonstrates that mineral dissolution begins before the formation of detectable clay minerals, establishing a fluid enriched in dissolved components. As temperature increases, continued dissolution enhances the concentration of these components, promoting supersaturation and enabling the nucleation of authigenic phases[25]. The preferential development of clay minerals on the grain surfaces indicates that detrital grains act as effective nucleation sites once favorable chemical conditions are reached. This marks a transition from dissolution-dominated processes to coupled dissolution–precipitation reactions, which control subsequent mineral evolution.

Overall, these observations show that small amounts of reactive minerals can exert a dominant influence on the diagenetic

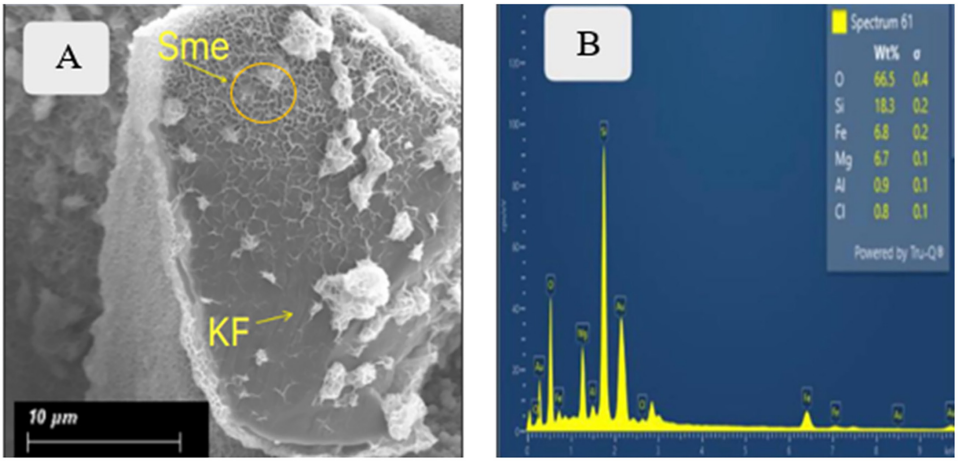


Figure 6. Scanning electron microscopy (SEM) and energy-dispersive spectroscopy (EDS) images displaying diagenetic features observed in Experiment 2 (150 °C). (*a*) SEM image showing the incipient precipitation of smectite (Sme) on the surface of a K-feldspar (KF) grain. (b) EDS spectrum from the clay-coated area (yellow circle in a) showing Al–Mg–Fe–bearing aluminosilicate minerals with minor amounts of Cl

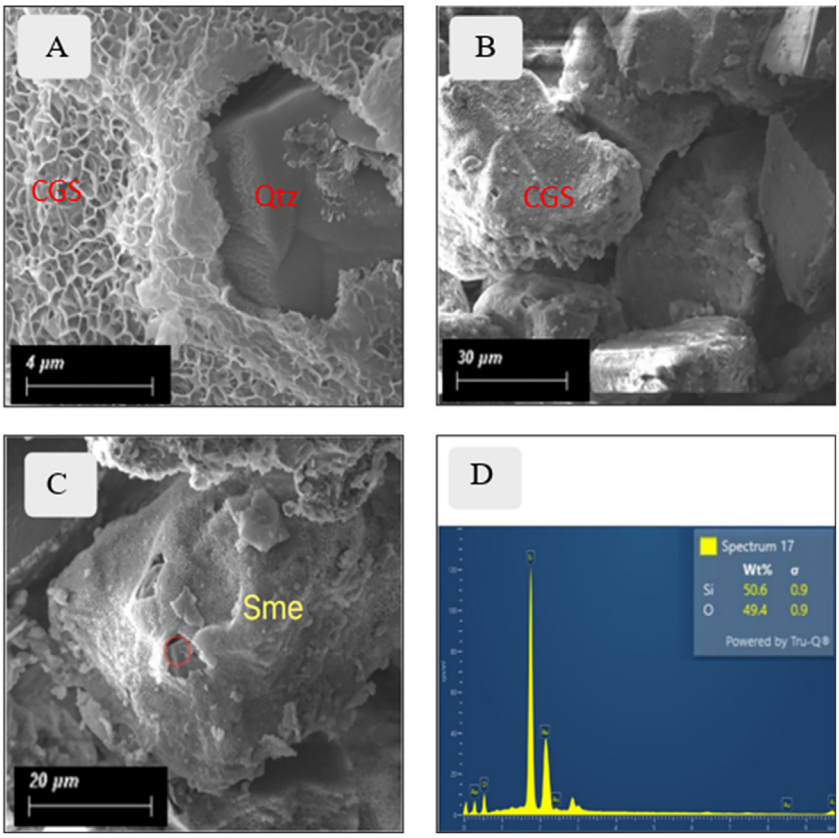


Figure 7. Scanning electron microscopy (SEM) and energy-dispersive spectroscopy (EDS) images displaying diagenetic features observed in Experiment 3 (200 °C). (a) High-magnification SEM image illustrating the thickness of the grain coating smectite (CGS), covering most of the detrital quartz (Qtz) grain. (b) SEM image showing multiple detrital grains mostly covered by smectite (CGS). (c) SEM image of a smectite (Sme) almost fully coating the grains, showing localized surface dissolution and pore development. (d) EDS spectrum from the clay-coated area (red circle in c) indicating a Si–O–rich composition consistent with authigenic aluminosilicate minerals

pathways in quartz-rich systems. This finding challenges the conventional assumption of chemical stability in quartz-dominated sandstones and underscores the importance of fluid–rock interactions in governing mineral transformation and reservoir evolution.

4.2. Formation and Transformation of Clay Minerals.

The experiments revealed a clear progression of clay mineral development with increasing temperature. Smectite first formed at 150 °C as discontinuous grain coatings, indicating the onset of authigenic clay precipitation. At 200 °C, these coatings became more extensive and better developed, suggesting enhanced reaction rates and increased availability of dissolved components. At higher temperatures (250 °C), the clay mineral assemblage shifted toward illite dominance. This transition reflects the progressive transformation of smectite into a more stable phase at elevated temperatures[26–28]. The preservation of the grain-coating geometry during this transition suggests that illite developed largely through the modification of pre-existing smectite rather than independent nucleation[29,30]. The transformation from smectite to illite is consistent with a temperature-controlled process influenced by the fluid composition[30,31]. Moreover, K availability plays a critical role in stabilizing the illite structure[15]. The experimental results indicate that K was supplied by both the dissolution of K-bearing minerals

Table 4. *Inductively coupled plasma–optical emission spectroscopy (ICP-OES) analysis results showing the concentrations of major ions in the solutions measured before and after the hydrothermal experiments (SM, Starting Material; ND, not detected)*

Identification		PH	TDS (ppm)	Major Ions (ppm)						
Experiment	Sample ID	PH	TDS	Na^{+}	K^{+}	Mg^{2+}	Ca^{2+}	Br^{+}	Li^{+}	Fe^{3+}
SM	GL0	8.05	70.60	5229.6	188.8	759.0	847.2	34.9	ND	5.86
Exp. 1	GL1	4.06	66.92	26989.7	1013.1	4352.7	1429.8	179.6	4.3	175.2
Exp. 2	GL2	4.32	64.46	14127.6	516.6	2081.9	1014.1	75.5	ND	152.7
Exp. 3	GL3	3.96	66.04	10184.7	410.9	1824.1	898.2	62.0	ND	373.0
Exp. 4	GL4	3.98	85.33	17430.7	1546.9	520.6	1632.4	77.6	3.6	2396.4

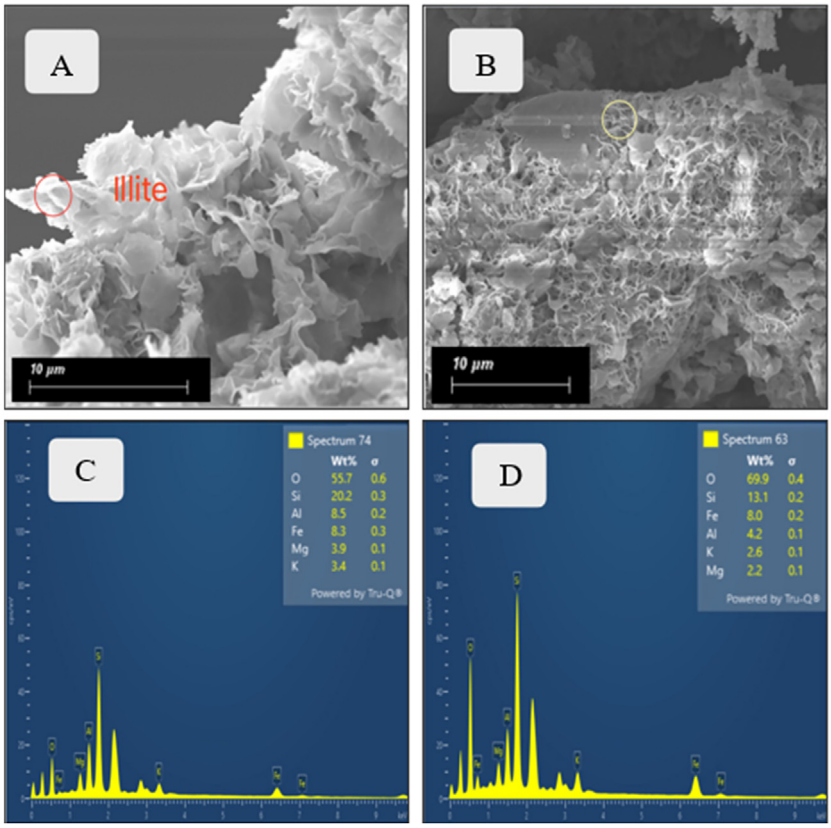


Figure 8. Scanning electron microscopy (SEM) and energy-dispersive spectroscopy (EDS) images displaying diagenetic features observed in Experiment 4 (250 °C). (a) SEM image of flocculated clay aggregates with irregular, sheet-like textures. (b) SEM image showing clay coatings developed on detrital grain surfaces. (*c*) EDS spectrum from the clay aggregate (red circle in a) indicating Al–Mg–Fe–K bearing aluminosilicate composition, typical of illite. (d) EDS spectrum from the clay-coated grain surface (yellow circle in b) showing Si–Al–Mg–Fe–K-rich clay mineral chemistry

and the reacting fluid, enabling the observed mineral transformation.

4.3. Coupling Between Mineral Evolution and Fluid Chemistry. The observed mineralogical changes are closely linked to variations in fluid composition, highlighting the importance of fluid–rock interactions during hydrothermal alteration. The decrease in dissolved Mg^{2+} with increasing temperature suggests its incorporation into the newly formed smectite, whereas the increase in Fe indicates continued release from dissolving mineral phases. Similarly, the increase in dissolved K^+ concentration reflects the ongoing dissolution of K-bearing minerals, particularly feldspar and mica. At higher temperatures, a portion of this dissolved K^+ is incorporated into illite, supporting the transformation. Thus, the evolution of the solid and fluid phases is strongly interconnected [32]. As the experiments were conducted in a closed system, the dissolved elements remained available for subsequent reactions. This enabled continuous redistribution of chemical components and facilitated the sequential development of smectite, followed by illitization. Therefore, the results demonstrate that mineral transformation in quartz-rich systems is governed by the dynamic exchange between the solid and fluid phases.

4.4. Implications for Reservoir Quality Evolution. The observed mineralogical and textural changes have direct implications for the evolution of reservoir quality in quartz-rich sandstones. The formation of smectite as a grain coating at moderate temperatures influences the pore structure by modifying the grain surfaces and inhibiting quartz cementation. Under certain conditions, such coatings may contribute to the preservation of the primary porosity [13,33]. However, continued diagenetic alteration leads to the transformation of smectite into illite, which is commonly associated with reduced permeability [34]. The platy and stacked morphology of the illite suggests that it can occupy pore space and restrict fluid flow. Therefore, the effect of clay minerals on reservoir quality evolves with temperature, shifting from beneficial to detrimental [24,34].

These findings highlight the importance of considering mineral transformation pathways when evaluating reservoir quality. Even in quartz-rich systems where chemical alteration is often underestimated, the presence of minor reactive minerals can initiate processes that significantly modify the pore structure during burial.

4.5. Limitations and Future Perspectives. Although these experiments provide valuable insights into the diagenetic processes, certain limitations should be acknowledged. The experimental duration was short relative to geological timescales, and elevated temperatures were used to accelerate the reactions. Consequently, the observed transformation pathways may not fully replicate the natural burial conditions. In addition, the experiments were conducted under closed-system conditions with a fixed fluid-to-solid ratio. Natural systems often involve

open fluid flows and variable geochemical conditions, which can influence mineral reactions and element transport.

Future work should focus on time-dependent experiments for a better constraint on the reaction kinetics, and advanced analytical techniques can further characterize clay mineral structures. Such studies would improve our understanding of mineral transformation processes and their impact on reservoir quality.

5. CONCLUSIONS

Considering a quartz-rich sand from the Middle Jurassic Mariedal Formation, southern Sweden, as our starting material, we investigated the diagenetic alteration pathways using controlled hydrothermal experiments designed to simulate burial conditions.

- This study demonstrated that, despite its apparent mineralogical simplicity, quartz-rich glass sand is not diagenetically inert. Even small proportions of reactive minerals, such as K-feldspar and muscovite, are sufficient for initiating and sustaining significant mineralogical transformations under hydrothermal conditions.
- Our experiments revealed a well-defined temperature-controlled alteration pathway. The initial feldspar dissolution occurred at low temperatures and provided the chemical components required for clay formation. Authigenic smectite developed at moderate temperatures as a grain-coating phase; upon further heating, it progressively transformed into illite. This confirms that clay mineral evolution in quartz-rich systems is governed by coupled temperature and fluid chemistry effects, particularly K availability.
- The results also highlight the strong coupling between solid-phase reactions and fluid composition. Systematic changes in Mg^{2+}, Fe^{3+}, and K^{+} concentrations demonstrate active element redistribution during alteration, emphasizing the role of fluid–rock interaction in controlling diagenetic processes.
- From a reservoir perspective, clay mineral evolution in quartz-rich sandstones is shown to significantly modify pore structure and flow properties. Early smectite coatings may influence cementation pathways, whereas later illitization may reduce permeability. These competing effects indicate that the evolution of reservoir quality is dynamic and closely linked to mineral transformation pathways.

In summary, these results have implications beyond hydrocarbon reservoirs, particularly for subsurface energy applications such as CO_2 storage and geothermal systems. The demonstrated sensitivity of quartz-rich sandstones to fluid–rock interactions suggests that mineral reactions and clay transformations must be considered when evaluating the long-term storage integrity and fluid flow behavior of subsurface reservoirs.

AFFILIATIONS AND AUTHOR DETAILS

Undergraduate Author

Ayah Alkhalifah – *Department of Geoscience, King Fahd University of Petroleum & Minerals, Dhahran 31261, Saudi Arabia*; 0009-0005-3358-2750
Email: s202469000@kfupm.edu.sa

Corresponding Author

Anas Muhammad Salisu – *Research Mentor, Research Scientist, Center for Integrative Petroleum Research, College of Petroleum Engineering and Geosciences, King Fahd University of Petroleum and Minerals*; 0009-0002-6134-0511
Email: anas.salisu@kfupm.edu.sa

ACKNOWLEDGEMENTS

The authors sincerely acknowledge the College of Petroleum Engineering and Geosciences (CPG) at King Fahd University of Petroleum and Minerals for providing the facilities and institutional support required for this study. We express our deep appreciation to Prof. Khalid Al-Ramadan for his guidance, constructive feedback, and continued encouragement throughout this study. We also thank Dr. Ayman Al-Leyhani for his valuable support and assistance during this study. We further acknowledge the contributions of Shahad Darwish, Fatimah Al-Ibrahim, Fatima AL-Shammary and Ayah Al-Aradi for their help during the fieldwork.

REFERENCES

(1) Barshep, D. & Worden, R. Reservoir Quality of Upper Jurassic Corallian Sandstones, Weald Basin, UK. *Geosciences (Basel).* **11**, 446 (2021).

(2) Worden, R. & Morad, S. Quartz Cementation in Oil Field Sandstones: A Review of the Key Controversies. *Spec. Publ. Int. Assoc. Sed.* **29**, 1–20 (2000).

(3) Khan, M. A., Khan, T., Ali, A., Bello, A. M. & Radwan, A. E. Role of depositional and diagenetic controls on reservoir quality of complex heterogenous tidal sandstone reservoirs: An example from the Lower Goru formation, Middle Indus Basin, Southwest Pakistan. *Mar. Pet. Geol.* **154**, 106337 (2023).

(4) McBride, E. F. Quartz cement in sandstones: a review. *Earth. Sci. Rev.* **26**, 69–112 (1989).

(5) Cook, J. E., Goodwin, L. B., Boutt, D. F. & Tobin, H. J. The effect of systematic diagenetic changes on the mechanical behavior of a quartz-cemented sandstone. *Geophysics* **80**, D145–D160 (2015).

(6) Haile, B. G., Hansen, H. N., Aagaard, P. & Jahren, J. How do chlorite coatings form on quartz surface? *J. Pet. Sci. Eng.* **215**, 110682 (2022).

(7) Alfaraj, M. A., Bello, A. M., Salisu, A. M. & Al-Ramadan, K. Kaolinite Illitization Under Hydrothermal Conditions: Experimental Insight into Transformation Pathways. *Minerals 2026, Vol. 16, Page 4* **16**, 4 (2025).

(8) Bello, A. M., Amao, A. O., Salisu, A. M. & Al-Ramadan, K. Clay-driven dolomitization at moderate to high temperatures: Evidence from hydrothermal experiments. *Geology* **53**, 1040–1045 (2025).

(9) Salisu, A. M., Bello, A. M., Amao, A. O. & Al-Ramadan, K. The Role of Fluid Chemistry in the Diagenetic Transformation of Detrital Clay Minerals: Experimental Insights from Modern Estuarine Sediments. *Minerals* vol. 15 Preprint at https://doi.org/10.3390/min15030317 (2025).

(10) Karpiński, B. & Szkodo, M. Clay Minerals – Mineralogy and Phenomenon of Clay Swelling in Oil & Gas Industry. *Advances in Materials Science* **15**, 37–55 (2015).

(11) Velde, B. Clay Minerals: A Physico-chemical explanation of their occurrence. *Developemnts in Sedimentology* 32–44 (1985).

(12) Worden, R. & Morad, S. Clay Minerals in Sandstones: Controls on Formation, Distribution and Evolution. in *Clay Mineral Cements in Sandstones* vol. 34 1–41 (2009).

(13) Walderhaug, O. & Porten, K. W. How Do Grain Coats Prevent Formation of Quartz Overgrowths? *Journal of Sedimentary Research* **92**, 988–1002 (2022).

(14) Ajdukiewicz, J. M. & Lander, R. H. Sandstone reservoir quality prediction: The state of the art. *American Association of Petroleum Geologists Bulletin* **94**, 1083–1091 (2010).

(15) Eberl, D. & Hower, J. The hydrothermal transformation of sodium and potassium smectite into mixed-layer clay. *Clays Clay Miner.* **25**, 215–227 (1977).

(16) Lahann, R. W. Smectite diagenesis and sandstone cement: the effect of reaction temperature. *J. Sediment. Petrol.* **50**, 755–760 (1980).

(17) Salisu, A. M., Bello, A. M., Amao, A. O., Lander, R. H. & Al-Ramadan, K. EXPERIMENTAL STUDY OF SMECTITE AUTHIGENESIS AND ITS SUBSEQUENT ILLITIZATION: INSIGHTS FROM MODERN ESTUARY SEDIMENTS. *Journal of Sedimentary Research* https://doi.org/10.2110/jsr.2024.135 (2025) doi:10.2110/jsr.2024.135.

(18) Al-Ramadan, K. Illitization of Smectite in Sandstones: The Permian Unayzah Reservoir, Saudi Arabia. *Arab. J. Sci. Eng.* **39**, 407–412 (2014).

(19) Saeed, M. Sedimentology and palynofacies analysis of Jurassic rocks Eriksdal, Skåne, Sweden. (Lund University, Lund, 2013).

(20) Krüger, A., Slater, S. & Vajda, V. 3D imaging of shark egg cases (Palaeoxyris) from Sweden with new insights into Early Jurassic shark ecology. *GFF* **143**, 229–247 (2021).

(21) Bello, A. M., Salisu, A. M. & Amao, Abduljamiu Olalekan, Umar, Mustapha, Al Ramadan, K. EXPERIMENTAL DEVELOPMENT OF CHLORITE: INSIGHTS FROM A KAOLINITE PRECURSOR. *Journal of Sedimentary Research* **95**, 1–24 (2025).

(22) Bello, A. M. *et al.* Experimental crystallization of analcime zeolite from clay and feldspar precursors. *Sci. Rep.* https://doi.org/10.1038/s41598-026-42250-3 (2026) doi:10.1038/s41598-026-42250-3.

(23) Khoshnaw, A. S., Alismail, D. N., Bello, A. M. & Al-Ramadan, K. Experimental Investigation of Kaolinite–Zeolite Transformation: Insights from Al-Habala Area Saprolite, Abha, Saudi Arabia. *Minerals 2025, Vol. 15, Page 920* **15**, 920 (2025).

(24) Bello, A. M., Al-Ramadan, K., Babalola, L. O., Alqubalee, A. & Amao, A. O. Impact of grain-coating illite in preventing quartz cementation: Example from permo-carboniferous sandstone, Central Saudi Arabia. *Mar. Pet. Geol.* **149**, (2023).

(25) Griffiths, J., Worden, R. H., Wooldridge, L. J., Utley, J. E. P. & Duller, R. A. Detrital Clay Coats, Clay Minerals, and Pyrite: A Modern Shallow-Core Analogue For Ancient and Deeply Buried Estuarine Sandstones. *Journal of Sedimentary Research* **88**, 1205–1237 (2018).

(26) Roberson, H. E. & Lahann, R. W. Smectite to Illite Conversion Rates: Effects of Solution Chemistry. *Clays Clay Miner.* **29**, 129–135 (1981).

(27) Inoue, A., KOHYAMA, N., KITAGAWA, R. & WATANABE, T. Chemical and Morphological Evidence for the Conversion of Smectite to Illite. *Clays and Clay Minerals - CLAYS CLAY MINER* **35**, 111–120 (1987).

(28) Mills, M. M. *et al.* Understanding smectite to illite transformation at elevated (>100 °C) temperature: Effects of liquid/solid ratio, interlayer cation, solution chemistry and reaction time. *Chem. Geol.* **615**, 121214 (2023).

(29) Haile, B. G., Hellevang, H., Aagaard, P. & Jahren, J. Experimental nucleation and growth of smectite and chlorite coatings on clean feldspar and quartz grain surfaces. *Mar. Pet. Geol.* **68**, 664–674 (2015).

(30) Lanson, B., Sakharov, B., Claret, F. & Drits, V. Diagenetic Smectite-to-Illite Transition in Clay-Rich Sediments: A Reappraisal of X-Ray Diffraction Results Using the Multi-Specimen Method. *Am. J. Sci.* **309**, 476–516 (2009).

(31) Lanson, B. *et al.* Authigenic kaolin and illitic minerals during burial diagenesis of sandstones: a review. *Clay Miner.* **37**, 1–22 (2002).

(32) Whitney, G. Role of Water in the Smectite-to-Illite Reaction. *Clays Clay Miner.* **38**, 343–350 (1990).

(33) Ajdukiewicz, J. M. & Larese, R. E. How clay grain coats inhibit quartz cement and preserve porosity in deeply buried sandstones: Observations and experiments. *Am. Assoc. Pet. Geol. Bull.* **96**, 2091–2119 (2012).

(34) Nadeau, P. H., Wilson, J., McHardy, W. J. & Tait, J. M. The Conversion of Smectite to Illite during Diagenesis: Evidence from some Illitic Clays from Bentonites and Sandstones. *Mineral. Mag.* **49**, 393–400 (1985).